Preparation of biomimetic hierarchically helical fiber actuators from carbon nanotubes

Jue Deng[1,2], Yifan Xu[1,2], Sisi He[1,2], Peining Chen[1], Luke Bao[1], Yajie Hu[1], Bingjie Wang[1], Xuemei Sun[1] & Huisheng Peng[1]

[1]Department of Macromolecular Science and Laboratory of Advanced Materials, State Key Laboratory of Molecular Engineering of Polymers, Fudan University, Shanghai, China. [2]These authors contributed equally to this work. Correspondence should be addressed to X.S. (sunxm@fudan.edu.cn) or H.P. (penghs@fudan.edu.cn).

Published online 8 June 2017; doi:10.1038/nprot.2017.038

Mechanically responsive materials that are able to sense and respond to external stimuli have important applications in soft robotics and the formation of artificial muscles, such as intelligent electronics, prosthetic limbs, comfort-adjusting textiles and miniature actuators for microfluidics. However, previous artificial muscles based on polymer materials are insufficient in generating large actuations, fast responses, diverse deformation modes and high cycle performances. To this end, carbon nanotubes (CNTs) are proposed as promising candidates to be assembled into artificial muscles, as they are lightweight, robust and have high surface-to-volume ratios. This protocol describes a reproducible biomimetic method for preparing a family of hierarchically arranged helical fiber (HHF) actuators that are responsive to solvents and vapors. These HHFs are produced through helical assembly of CNTs into primary fibers and further twisting of the multi-ply primary fibers into a helical structure. A large number of nanoscale gaps between the CNTs and micron-scale gaps between the primary fibers ensure large volume changes and fast responses upon the infiltration of solvents and vapors (e.g., water, ethanol, acetone and dichloromethane) by capillarity. The modes of shape transformations can be modulated precisely by controlling how the CNTs are assembled into primary fibers, multi-ply primary fibers, HHFs and hierarchical springs. This protocol provides a prototype for preparing actuators with different fiber components. The overall time required for the preparation of HHF actuators is 17 h.

INTRODUCTION

The emergence of mechanically responsive materials that can sense and respond to external stimuli has attracted broad interest in fundamental research; such materials have various applications, including use in the formation of artificial muscles[1,2] and soft robotics[3,4]. The essential principle of engineering shape transformations is to design anisotropic atomic or molecular structures. Many kinds of responsive materials have been developed by following this structure–function relationship, including azobenzene-based liquid crystal elastomers[5] and asymmetric hydrogels[6]. The formation of helical structures is an important strategy for introducing anisotropic units[7–10]. This strategy has been frequently found in biological materials and contributes to complex mechanical functions such as asymmetry of growth, anisotropy of swelling, disparity of surface stress and other geometric properties[2,11]. For example, awns drill themselves into the ground by repeatedly curling and unwinding a spiral shape[12], and seed pods twist themselves to open[13].

Inspired by the helical structures in plants, a variety of mechanically responsive materials have been explored. By mimicking the cellulose fibrils of plants, materials such as synthetic polymers[14,15], nanowires[16] and CNTs[17] have been helically assembled to realize shape transformations. Creation of a spiral across the thickness of a synthetic liquid crystal polymer film is used to form programmable helical actuators. However, the difficulty for scientists in accessing high-intensity UV light in practical applications and the rigorous requirement for chemical synthetic processes have limited the applications of liquid crystalline polymers[14,18]. CNTs and nanowires that are twisted to form yarns or helically wound on the surfaces of polymer fibers are able to produce rotary and contractive actuations during the volume change caused by electrochemical and thermal stimuli[19–22]. These responsive materials based on simple helical organization exhibited relatively poor actuation performances, such as slow response and small deformation.

Designing a hierarchy of helical structures from the nanoscale to the macroscopic scale promises to be an effective strategy for preparing responsive materials that can undergo highly efficient mechanical motion. Some plant parts, such as a tendril, exhibit hierarchically helical structures used to produce rapid and tunable mechanical actuations (**Fig. 1**). This provides a new inspiration for designing high-performance actuators with multilevel helical structures[8,23]. The strategy described here is for

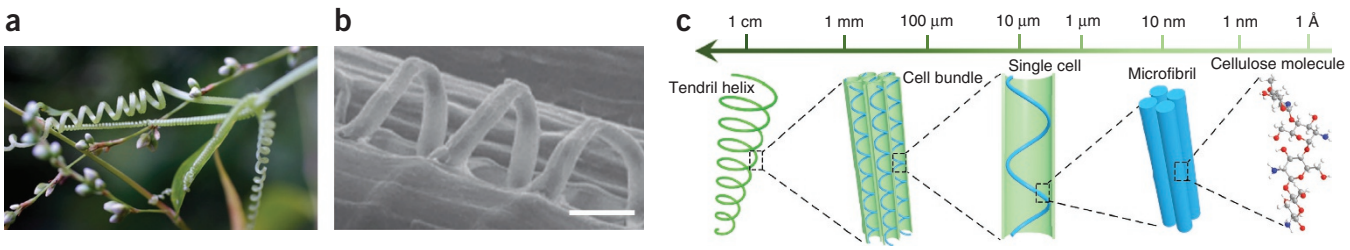

Figure 1 | A hierarchically helical structure of Towel Gourd tendrils. (**a**) Tendril helices with hooking. (**b**) A single cellulose helix in the tendril filaments. Scale bar, 10 µm. Image reproduced with permission from ref. 23, Macmillan Publishers. (**c**) Hierarchical arrangement of a tendril helix, sequentially built from bundles of cells containing cellulose helices made from cellulose molecules.

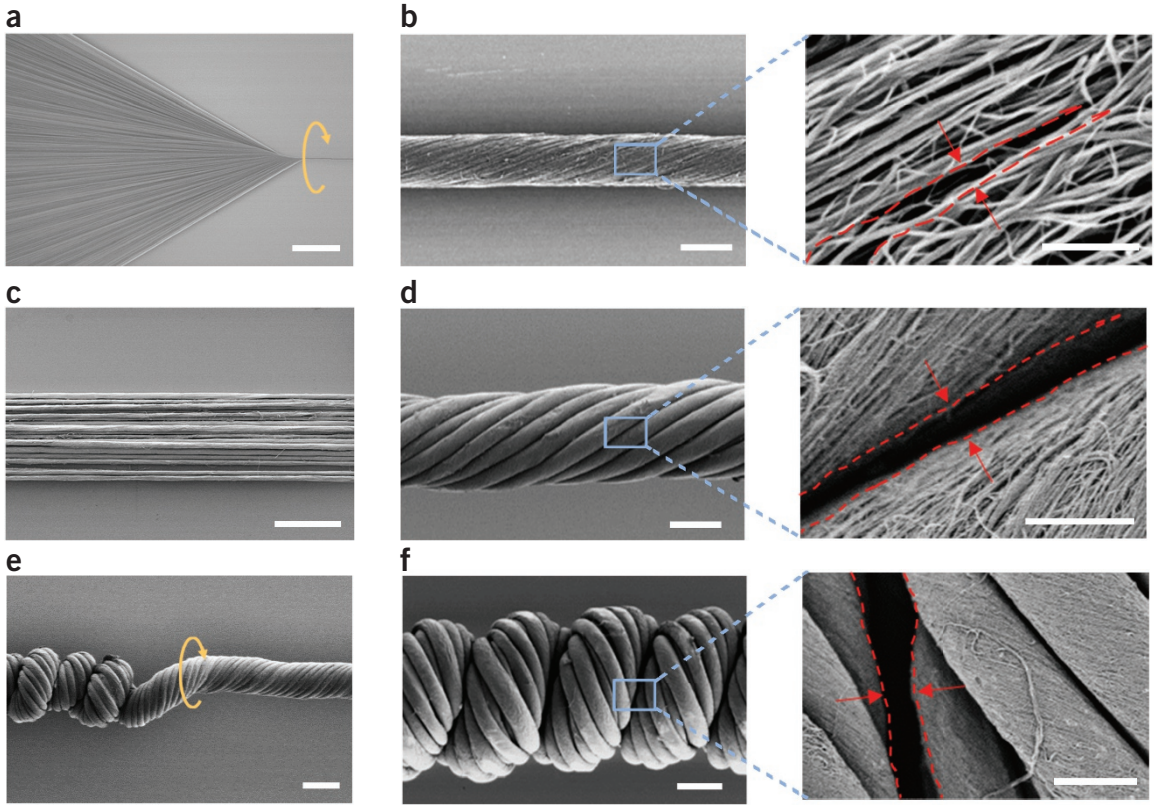

Figure 2 | Formation of the HHF with multiscale gaps. (**a**) SEM image of an aligned CNT sheet being twisted into a helical primary fiber. Scale bar, 500 μm. (**b**, left) A primary fiber with a helical angle of 32°. Scale bar, 10 μm. (**b**, right) Enlarged view of boxed region in left-hand panel. The red lines show a nanoscale gap between neighboring CNTs. Scale bar, 500 nm. (**c**) Multi-ply primary fibers arranged in parallel. Scale bar, 200 μm. (**d**, left) Twisted primary fibers. Scale bar, 30 μm. (**d**, right) Enlarged view of boxed region in left-hand panel. The red lines show a micrometer-scale gap among two neighboring primary fibers. Scale bar, 2 μm. (**e**) Overtwisting the primary fiber with coils gradually formed along the axial direction of the fiber. Scale bar, 50 μm. (**f**, left) SEM image of the HHF. Scale bar, 30 μm. (**f**, right) Enlarged view of boxed region in left-hand panel. The red lines show a coiled gap. Scale bar, 10 μm. **b**, **d** and **f** adapted with permission from ref. 24, Nature Publishing Group. SEM, scanning electron microscopy.

preparing HHFs that respond to solvent and vapor stimuli. HHFs are produced by dry-spinning primary fibers from CNT arrays and then twisting the multi-ply primary fibers into a helical structure[24,25]. The resulting HHFs provide a large number of nanoscale gaps between the helically aligned CNTs and micrometer-scale gaps between neighboring primary fibers, contributing to a rapid response and a large actuation stroke in response to solvents and vapors. The HHFs produced in this protocol are porous, lightweight, flexible, stretchable and mechanically strong, and thus they exhibit promising applications in a variety of fields[26,27], such as artificial muscles that provide damaged limbs with the capability of dynamic motions similar to those of natural human muscles and soft sensors that can be easily integrated into flexible, elastomeric and even wearable electronic devices.

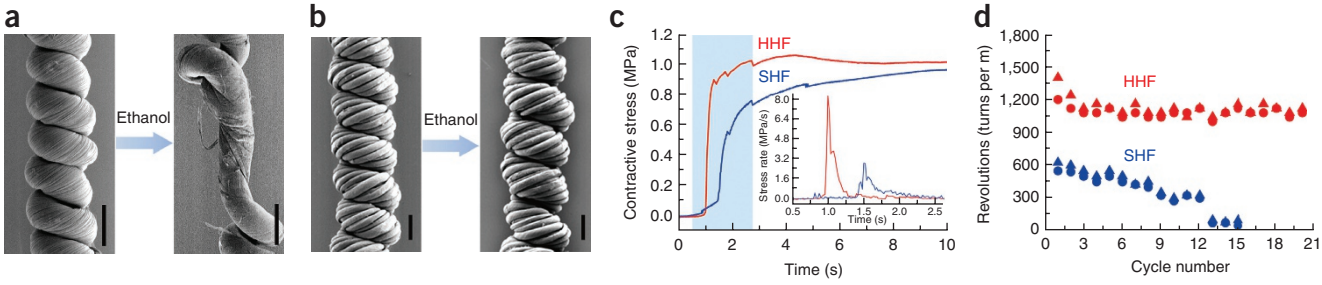

Figure 3 | Actuation performance of helical fibers. (**a**) SEM images of a single-ply helical fiber twisted from stacked multi-ply CNT sheets before (left) and after (right) infiltration of ethanol. The helices become untwisted because of the unstable structure during the actuation. Scale bars, 100 μm. (**b**) SEM images of an HHF before (left) and after (right) infiltration with ethanol. The structure is well maintained after actuation. Scale bars, 100 μm. (**c**) Dependence of the contractive stress on the time for the HHF (red line) and SHF (blue line). (**d**) Dependence of the speed of revolution on the cycle number for the HHF (red dots) and SHF (blue dots) in the forward (triangles) and reverse (circles) rotations. SEM, scanning electron microscopy. Images adapted with permission from ref. 24, Nature Publishing Group.

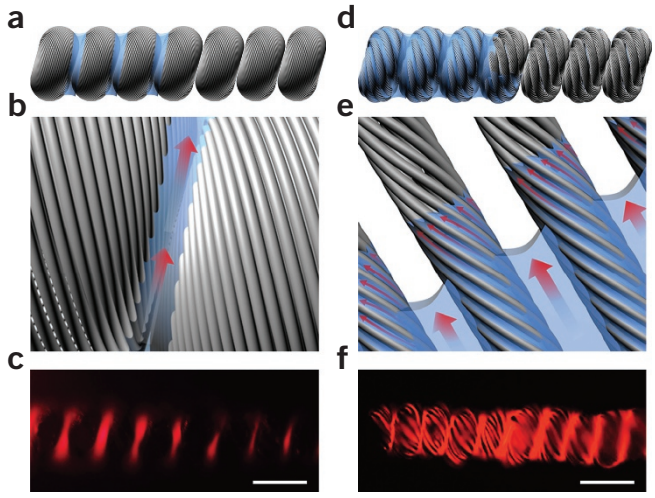

Figure 4 | Hierarchically arranged gaps formed in the helical fibers. (**a**) Schematic illustration of the infiltration of solution along an SHF. (**b**) Enlarged schematic illustration of the infiltration through the micrometer-scale gap (arrows) between the adjacent coils. (**c**) Fluorescence micrograph of the SHF after coming into contact with a rhodamine–ethanol solution. Scale bar, 100 μm. (**d**) Schematic illustration of an HHF upon infiltration of solution. (**e**) Enlarged schematic illustration of the infiltration through the nanometer-scale gaps (small arrows) among the aligned CNTs and micrometer-scale gaps among primary fibers (big arrows). (**f**) Fluorescence micrograph of the HHF after coming into contact with a rhodamine–ethanol solution. Scale bar, 100 μm. **c**,**e**,**f** adapted with permission from ref. 24, Nature Publishing Group.

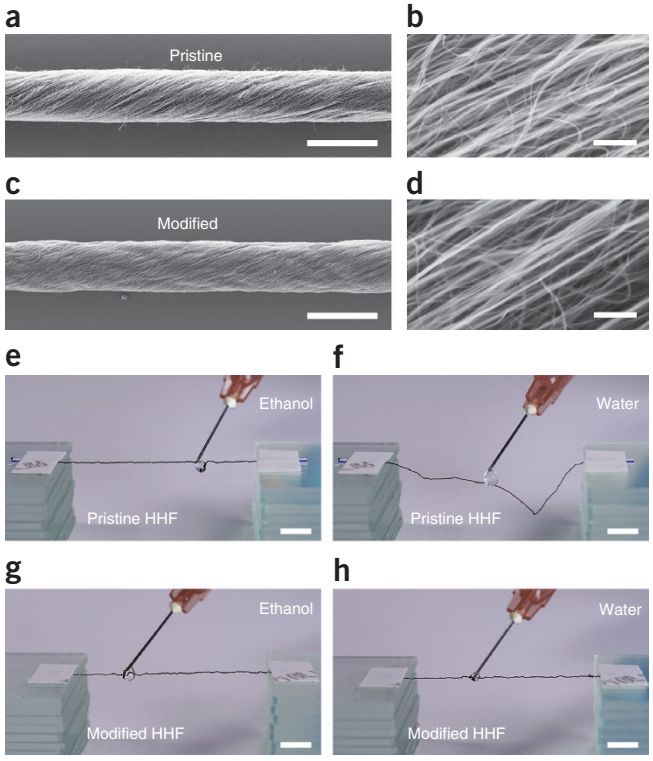

Figure 5 | The comparison of actuation performance of pristine HHFs and modified hydrophilic HHFs. (**a**,**b**) SEM images of the primary CNT fiber at (**a**) low and (**b**) high magnifications. Scale bars, 20 μm (**a**); 400 nm (**b**). (**c**,**d**) SEM images of the modified fiber at (**c**) low and (**d**) high magnifications. Scale bars, 20 μm (**c**); 400 nm (**d**). (**e**,**f**) Actuation performance of pristine HHFs in response to (**e**) ethanol and (**f**) water. No response is available for water. Scale bars, 0.5 cm. (**g**,**h**) Actuation performance of modified hydrophilic HHFs in response to (**g**) ethanol and (**h**) water. Hydrophilic HHFs show contractive actuations to both ethanol and water. Scale bars, 0.5 cm. SEM, scanning electron microscopy. **a**–**d** adapted with permission from ref. 25, Wiley.

Development of the protocol

The applications in artificial muscle formation and soft robotics require high rotation output, rapid responsiveness, high reversibility and good controllability. To achieve these goals, we developed this protocol by designing hierarchically helical CNT structures to amplify the actuating performance in rotation and contraction. On the basis of the combined excellent properties of being lightweight and robust, and having high surface-to-volume ratios, CNTs are promising candidates for the generation of artificial muscles. In addition, CNTs exhibit better performance in both actuation rate and lifetime as compared with polymer muscles[28,29]. CNTs were helically assembled into primary fibers for the first time >10 years ago[30]. These helically assembled CNT artificial muscles—which work on the basis of volume expansion caused by the injection of large ions into electrodes—demonstrated much higher actuation stresses than natural muscles did[31]. However, these actuations generally required extremely high voltages for giant strains[32], and it remains challenging to amplify the strains to satisfy practical applications. We demonstrated a new and promising strategy for generating the desired dimensional changes by infiltration of solvents or vapors[24] instead of injection of large ions into electrodes[31]. The designed hierarchically helical structure with nanometer- and micrometer-size gaps greatly enhanced the actuation performance. The modes of the mechanical motions are tunable and programmable by varying the specifics of the helical structure, such as the degree of helical angles, the number of primary fibers and helix-chiral morphology. This protocol can be generalized for various nanomaterials that can form primary fibers, such as graphene oxide and polymers, which are responsive to a spectrum of solvents and vapors.

Experimental design

Production of hierarchical structures using a twisting process. In this protocol, we take advantage of the high surface area and superb mechanical properties of the aligned CNTs to fabricate porous, lightweight, flexible and strong fiber actuators. The aligned CNTs are first spun from the CNT array grown by chemical vapor deposition and twisted together to form primary fibers (**Fig. 2a**). Many nanometer gaps are formed along the aligned CNTs (**Fig. 2b**). Many parallel primary fibers are then packed (**Fig. 2c**) and twisted into a helical structure (**Fig. 2d**, left). Micrometer-scale gaps are formed among the adjacent parallel primary fibers (**Fig. 2d**, right). During the further twisting process, many coils are gradually formed when the rotation angle exceeds a critical point (**Fig. 2e**). Finally, freestanding HHFs are prepared after the creation of compact coils along the longitudinal direction, with larger coiled gaps between the neighboring helical coils (**Fig. 2f**).

The hierarchical structure enhances actuating properties. The hierarchical arrangement of CNTs and the resulting gaps between the fibers have important roles in the actuation. For comparison, a single-ply helical fiber (SHF) with a coiled structure is twisted from stacked multilayer CNT sheets, with a similar amount of CNTs but without the hierarchically helical structure. For the

SHFs, nanoscale and coiled gaps are generated from the aligned CNTs and neighboring coils, respectively (**Fig. 3**). Although both HHFs and SHFs can produce contraction and rotation in response to solvents, the stress rate and the rotary actuation revolution speeds of HHFs are substantially higher than those generated by the SHFs (**Fig. 3**). Besides, the revolution speeds of the SHFs decrease markedly with partial untwisting of the coils after 15 cycles of ethanol infiltration, whereas the HHFs exhibit a high stability in both structure and actuation. In general, volume expansion is a critical factor in the actuation of torsional fiber actuators. The difference in actuation between the HHFs and SHFs could be attributed to different gap structures, resulting in different infiltration behaviors of solvents driven by capillary forces[33] (**Fig. 4**). For the SHFs, nanoscale helical gaps are mainly formed in the CNT coils, and only a small amount of rhodamine–ethanol solution (concentration of 0.1 mg/ml) was found in the gaps between neighboring coils (**Fig. 4a–c**). By contrast, hierarchical gaps at both the nanometer and micrometer scales were formed in the coils of the HHFs. As compared with the SHFs, the additional gaps of the HHFs provide a higher capacity for solvent infiltration, so a larger amount of free energy will be released from the surface and turned into actuation energy. This generates a more rapid and efficient volume expansion with a faster response (**Fig. 4**). In addition to the higher expansion, the larger actuation stroke in the HHFs may also be attributed to the larger number of twisted turns in the preparation. It was calculated that the number of twisted turns stored in the HHFs was >30 times that in the SHFs[24]. The HHFs can further perform large contractions and elongations in response to vapors after being shaped into springs.

Hydrophilic modification of CNTs, enabling actuations in response to water. To expand the range of applications, the resulting primary CNT fiber can be modified to be hydrophilic through an oxygen plasma treatment. In comparison with the other modification methods[34,35], no obvious damage to the helical structure was observed after oxygen plasma treatment. The multiple gaps between the CNTs are properly maintained (**Fig. 5a–d**). In particular, the modified hydrophilic HHF is equally efficient as pristine HHF in contraction movement after the adsorption of water. The as-prepared hydrophobic HHFs rapidly respond to ethanol but do not exhibit actuations in water (**Fig. 5e–h**). The hydrophilic fiber responds to water with a longitudinal contraction of ~20% within 90 ms. This response is faster than that of a Venus flytrap (~200 ms)[36], which produces the fastest movement in plants. The midpoint of the hydrophilic fiber produces a maximal ascending velocity of 0.12 m/s during the initial 33.3 ms. Moreover, the contractive stress generated by the hydrophilic fiber is almost three times the stress generated by a hydrophobic fiber in response to ethanol.

MATERIALS

REAGENTS

- Silicon wafer (d = 100 mm, h = 510 µm, containing a silica surface of 3,000-nm thickness; Tianjin Crystal Lattice Photoelectric Material, cat. no. BC-12-C328-LC)
- Aluminum oxide (99.995% (wt/wt); Shanghai Institute of Optics and Fine Mechanics)
- Iron (99.99% (wt/wt); Shanghai Institute of Optics and Fine Mechanics)
- Hydrogen gas (≥99.999% (vol/vol); Shanghai Tomoe Gases)
  ! CAUTION Hydrogen gas is dangerous. Prevent any leakage and keep it away from open flame.
- Argon gas (≥99.999% (vol/vol); Shanghai Tomoe Gases)
- Ethylene gas (≥99.999% (vol/vol); Shanghai Tomoe Gases)
  ! CAUTION Ethylene gas is dangerous. Prevent any leakage and keep it away from open flame **▲ CRITICAL** Use high-purity hydrogen, argon and ethylene gases.
- Absolute ethyl alcohol (≥99.7% (wt/wt); Sinopharm Chemical Reagent Co., cat. no. 10009218)
- Silver paste (silver conductive paint; SPI Supplies, cat. no. 04998-AB)
- Rhodamine (Rhodamine 6G; J&K Scientific)
- Quartz tube (d = 2.5 and 5 cm; Hefei Ke Jing Materials Technology)
- Quartz boat (l = 10 cm, w = 17 mm, h = 10 mm; Hefei Ke Jing Materials Technology)
- Copper paddle (Sigma-Aldrich, cat. no. GF21550890)
- Vinyl electrical tape (3M, cat. no. 1700-3/4×60FT)
- Double-sided adhesive tape (3M, cat. no. 3M908)
- Polyimide double-sided adhesive tape (3M, cat. no. 3M92)

EQUIPMENT

- Electron beam evaporation coating system (SKY Technology Development, cat. no. DZS-500)
- Tube furnace (Hefei Ke Jing Materials Technology, cat. no. OTF-1200X)
- Muffle furnace (Thermo Fisher Scientific, cat. no. HTF55322C)
- Table-top Universal Testing Instrument (HY0350; Shanghai HengYi Precision Instrument)
- Servo motor (Deou Electric Technology, cat. no. DO-1000B)
- Stepping motor (Xiner Electric, cat. no. MTPG2)
- Field-emission scanning electron microscopy (Zeiss, model no. Ultra 55)
- Digital camera (Nikon, model no. J1)
- Oxygen microwave plasma (PVA Tepla, model no. Plasma System 690)
- Drop shape analyzer (Dataphysics, model no. OCA 40)
- Optical microscope (Olympus, model no. BX51)
- Diamond cutter (Zhejiang Li Jing Photovoltaic-Tech, model no. D-100)

PROCEDURE

Preparation of CNT arrays ● TIMING 7 h

1| Remove dust from the silicon wafer by ushing it with a nitrogen stream before use.

2| Place the target materials (aluminum oxide and iron) into two different copper crucibles at the bottom of the electron beam evaporation coating system's chamber, and place the silicon wafer over the target materials (with the polished surface downward). Close the shutter before deposition.

3| Vacuum the chamber to 5×10^{-4} Pa for appropriately 2 h.

4| Switch the target material to aluminum oxide, and open the high-energy electron beam to evaporate the aluminum oxide. After the deposition rate is stabilized at 2 Å/s, open the shutter and start the deposition of aluminum oxide. Close the shutter and turn off the high-energy electron beam once the thickness of aluminum oxide reaches 3 nm.

5| Switch the target material to iron, and open the high-energy electron beam to evaporate the iron. Once the deposition rate is stabilized, deposit the iron on the silicon wafer at a deposition rate of 0.5 Å/s. The desired thickness of iron is 1.2 nm.
▲ **CRITICAL STEP** Nonuniform and inappropriate thickness of aluminum oxide or iron can decrease the spinnability of the CNT array.
? TROUBLESHOOTING

6| Exhaust the chamber to atmospheric pressure, and take the silicon wafer from the chamber.

7| Cut the silicon wafer into a size of 1.2 × 2.5 cm using a diamond cutter, and remove any fragments produced during the cutting process by ushing the wafer with a nitrogen stream. The size of the resulting silicon wafer is determined by the diameter of the quartz tube used. The width of the silicon wafer should be smaller than the diameter of the quartz tube.
▲ **CRITICAL STEP** Any remaining fragments can prevent the growth of CNTs in the following step.

8| Place the silicon wafer in the middle of a tube furnace (diameter of 5.08 cm) and remove the air in the tube furnace by flowing argon gas at a rate of 400 s.c.c.m. for 8 min (**Supplementary Fig. 1**).
▲ **CRITICAL STEP** Residual oxygen and water in the air can affect the spinnability of CNT array.

9| Flow hydrogen and ethylene gas into the tube at rates of 30 and 90 s.c.c.m., respectively. At the same time, increase the temperature to 740 °C over 15 min.

10| Maintain the temperature at 740 °C for 10 min.

11| Stop the flow of hydrogen and ethylene gas, and cool the tube down to below 100 °C (typically, at a cooling speed of ~10 °C/min). Note that the cooling speed does not obviously affect the quality of the synthesized CNT array. Open the quartz tube and remove the silicon wafer with the CNT array grown on it.
! CAUTION Make sure that the tube furnace has been cooled down to a relatively low temperature before you open it.
▲ **CRITICAL STEP** Keep flowing argon gas through the quartz tube to prevent backflow of the sealing liquid during the cooling process.
? TROUBLESHOOTING

Preparation of HHFs ● TIMING 3 h

12| Stick the resulting CNT array to the rotor of a servo motor using double-sided adhesive tape, pull out the CNT sheet from the array and fasten one end of the sheet to a collecting drum of a stepping motor using a small piece of vinyl electrical tape (**Supplementary Fig. 2a**).
▲ **CRITICAL STEP** The CNT sheet should be positioned horizontally and at the same height as the upper surface of the collecting drum to guarantee a continuous dry-spinning process.

13| Dry-spin the primary fibers from the CNT array. The primary fibers here are left-handed after counterclockwise twisting of the servo motor and clockwise twisting of the collecting motor (**Supplementary Fig. 2b**). The helical angles of the primary fibers can be increased from 8°, 16°, 32° and 37° to 43° and are controlled by increasing rotation speeds from 500, 1,000, 2,000 and 2,500 to 3,000 r.p.m., respectively. Draw the nonhelical primary fibers directly out of the array without rotation, followed by passing them through a small pipe filled with alcohol to shrink them. The collecting speed of primary fibers is 8 m/h. An optimal helical angle of 32° is typically used because it yields the largest contractive stress generation.
▲ **CRITICAL STEP** The distance between the servo and stepping motors should be <20 cm; longer distances may greatly decrease the stability of the dry-spinning process.
▲ **CRITICAL STEP** The diameters of primary fibers can be increase from 10.3, 15.0 and 20.4 to 24.7 μm, and are controlled by increasing the width of the CNT array from 0.5, 1.0 and 1.5 to 2.0 cm, respectively. We use the primary fibers with a diameter of 15 μm for the following experiments.
■ **PAUSE POINT** CNT arrays and fibers can be stored in a dry and dust-free container at room temperature (25 °C) for several months without obvious changes in spinnability and other properties.

14| Arrange 20-ply primary fibers with a length of 25 cm in parallel, and fix them on a clean sheet of paper with vinyl electrical tape to stabilize the two ends (**Supplementary Fig. 3a**).
▲ **CRITICAL STEP** The primary fibers should be uniform in diameter. Large fluctuations in the diameters of the primary fibers may result in their untwisting at a high cycle number.

15| Assemble the primary fibers together and stabilize the overlapping ends with additional vinyl electrical tape (**Supplementary Fig. 3b**). Cut the paper to make it 30 cm in length and 3 cm in width.
▲ **CRITICAL STEP** Keep the fibers straight and aligned to ensure uniformity of the formed HHFs.
▲ **CRITICAL STEP** Make sure that the two ends of the fibers are stabilized properly; otherwise, they will intertwine.
? TROUBLESHOOTING

16| Clamp one end of the aligned primary fibers to a rotating motor shaft while keeping the other end attached to the paper slip. Attach the paper slip with a length of 8 cm to a movable substrate—e.g., a book or a box (**Supplementary Fig. 4a**). Cut off the spare paper and position the substrate so that the fiber is horizontal and straight. Ensure that the two ends of the paper slip are tightly fastened to the motor shaft (**Supplementary Fig. 4b**).
▲ **CRITICAL STEP** The weight of the paper slip is ~170 mg, which is critical to the preparation of HHFs. If the paper slip is too light, the applied force will not be enough to stretch the fiber; if the paper slip is too heavy, the applied force will be too high and the fiber will break easily.
▲ **CRITICAL STEP** Make sure that the ends are fastened tightly enough; otherwise, the fiber will tangle into a mess.

17| Rotate the motor at a speed of 200 r.p.m. in a counterclockwise direction. During the twisting process, maintain the fibers in a horizontal position and keep them straight by moving the substrate toward the motor. The HHF here is left-handed. The first coil is formed when the number of turns exceeds a critical point, and the coils are created sequentially along the axial direction (**Supplementary Fig. 4c,d**).
▲ **CRITICAL STEP** Properly control the moving speed of the substrate to keep the fibers straight. The moving speed of the substrate should be ~2.5 cm/min. If the substrate moves too quickly, it is easy for the fibers to become tangled; if the substrate moves too slowly, the fibers tend to break.

18| Stop the twisting process once the diameter of the whole fiber becomes uniform. The resulting fiber is found to form a looped structure.

19| Apply ethanol to the fiber using a syringe, and then untwist the fiber in the opposite direction to release the excessive twisting (**Supplementary Fig. 5**).

20| Stop the untwisting process when the freestanding fiber is not entangled anymore.
? TROUBLESHOOTING

21| Use a tweezers to carefully remove the end of the fiber from the motor without stretching the fiber, and fasten it to the paper slip using vinyl electrical tape. A freestanding HHF with a length of ~6 cm is obtained. The density of the HHF is 0.54 g/cm^3.
▲ **CRITICAL STEP** Excessive stretching of the fiber can cause untwisting. The two ends of the fiber should be moved close to each other before taking the end away from the motor.

Preparation of SHFs ● TIMING 1 h
22| Stack 20 layers of CNT sheets with the same width (1 cm) and length (25 cm) together. Fasten one end to a stabilized paper and the other to the rotating motor shaft.

23| Rotate the motor at a speed of 200 r.p.m. for 10 s.

24| Repeat Steps 16–21.

Preparation of a spring fiber ● TIMING 2 h
25| Prepare the spring fiber by a thermo-hydro setting method. Wrap an HHF around a glass rod to form a spring, and fasten the two ends with polyimide double-sided adhesive tape (**Supplementary Fig. 6a**).
▲ **CRITICAL STEP** The setting process occurs at a relatively high temperature; common adhesive tape cannot withstand such a temperature and thus should not be used. We therefore recommend using polyimide double-sided adhesive tape.

© 2017 Macmillan Publishers Limited, part of Springer Nature. All rights reserved.

26| Place the glass rod in a muffle furnace (diameter of 2.54 cm) and remove the air from the furnace tube by flowing argon gas at a rate of 400 s.c.c.m. for 8 min (**Supplementary Fig. 6b,c**).

27| Heat the muffle furnace to 300 °C for 1 h to set the HHF.
▲ **CRITICAL STEP** If the fiber becomes separated from the adhesive tape or if the fiber released from the glass rod does not take the desired helical shape, repeat the Steps 25–27 with the same HHF.

Preparation of hydrophilic fibers ● TIMING 2 h
28| Spin the primary CNT fibers on a rotating drum and arrange them at regular intervals (**Supplementary Fig. 7a**).
▲ **CRITICAL STEP** Avoid overlapping of the fibers, which may cause inhomogeneity in the following treatment.

29| Treat the fibers with oxygen microwave plasma at a pressure of 0.1 mbar and a flow rate of oxygen gas of 300 s.c.c.m. (**Supplementary Fig. 7b**). Treat the fibers at 100 W for 15 min. The treatment does not produce obvious damage to the nanoscale gaps among the neighboring CNTs (**Fig. 5a–d**).
■ **PAUSE POINT** The resulting hydrophilic fibers can be stored at room temperature for several months without obvious changes in properties.

30| Test the effect of the oxygen plasma treatment using contact angle measurement. Place the treated sample on a table with a syringe containing water. Extrude a water droplet from the syringe, and keep it at the top of the needle. Bring the needle into close proximity to the sample, until the water droplet comes into contact with the sample (**Supplementary Fig. 8**). The contact angle between the sample and the water droplet can thus be measured.

Rotary actuation of fibers ● TIMING 1 h
31| Label the two sides of a copper paddle with two pieces of differently colored tape. These pieces of tape are used as the reference to measure the rotatory angle (**Fig. 6a,b**).

32| Fasten one end of the fiber to the paddle and the other end to a hung cantilever. Place a camera and a needle with tested solution (water or absolute ethyl alcohol) beside the fiber. Here, the mass of the paddle is 75 mg and the length of the fiber is 2 cm.
▲ **CRITICAL STEP** The end of the fiber should be fastened to the middle of the paddle to make the paddle horizontal for convenient measurement.

33| Focus the camera on the fiber.

34| Extrude a solution droplet from the syringe and bring the needle into close proximity to the fiber.
▲ **CRITICAL STEP** Use a needle of the same size for each experiment to ensure the same volume of droplet.

35| Record a high-speed video (400 frames per s).

36| Analyze the revolution speed of the rotor by examining the video frame-by-frame. The revolution speed of the rotor (θ) is determined by the equation $\theta = 90° - \arcsin(d/l)$, where l and d correspond to the actual and projected lengths of the copper paddle, respectively (**Supplementary Fig. 9**).

Contractive actuation of fibers ● TIMING 1 h
37| Cut a square hole with a sides of 1.5 cm in a piece of paper, and fix the two ends of the fiber to the paper over the hole by using silver paste (**Supplementary Fig. 10a,b**).
▲ **CRITICAL STEP** The hole should be wide enough to prevent breaking the fiber in the following cutting process.

38| Clamp the two ends of the fiber onto two grids of a Table-top Universal Testing Instrument, and then cut the part of the paper that is not in the clamps (marked by the dashed line; **Supplementary Fig. 10b,c**). Apply a stress of appropriately 1.5 MPa.

39| Apply a droplet of ethanol to the fibers using a syringe (**Supplementary Fig. 10c**) and measure the solvent-induced contractive force using the Table-top Universal Testing Instrument.

? TROUBLESHOOTING
Troubleshooting advice can be found in **Table 1**.

TABLE 1 | Troubleshooting table.

Step	Problem	Possible reason	Solution
5	Nonuniform or inappropriate thickness of aluminum oxide or iron	Large fluctuation in deposition rate during deposition	Ensure that the electron beam irradiates at the center of the target materials, and do not start deposition until the depositing rate is stable
11	The CNT array shows poor spinnability	(i) There is too much carbon residue in the tube furnace after a long period of growth	(i) Burn the tube furnace in air at 750 °C for 10 min
		(ii) The temperature is unstable during the growing process	(ii) Preheat the tube furnace. Check the temperature control system. Use asbestos to seal the two ends of the tube furnace to avoid uneven temperature in the tube furnace
		(iii) The exhaust gas is hindered because of too much carbon residue in the exhaust pipe, which causes high internal pressure in the tube furnace	(iii) Clean the exhaust passage
15	Some primary fibers are separated from the multi-ply primary fiber, although the two ends have been fastened	Some primary fibers were not straightened properly during the arrangement of the multi-ply fiber, so they are longer than the others	Carefully use the tweezers to make these fibers straight, with any extra part being moved to the end
20	The resulting HHFs are inhomogeneous	They were not properly maintained in a horizontal position during the twisting process	Untwist the HHF by changing the twisting direction of the servo motor, followed by carefully aligning the inhomogeneous parts and retwisting the fibers while ensuring that they are positioned horizontally

● TIMING

Steps 1–11, preparation of CNT arrays: 7 h
Steps 12–21, preparation of HHFs: 3 h
Steps 22–24, preparation of SHFs: 1 h
Steps 25–27, preparation of a spring fiber: 2 h
Steps 28–30, preparation of hydrophilic fibers: 2 h
Steps 31–36, rotary actuation of fibers: 1 h
Steps 37–39, contractive actuation of fibers: 1 h

ANTICIPATED RESULTS

The protocol can be used to prepare single primary fibers, HHFs and springs based on the HHFs (**Fig. 6**). These fiber materials should exhibit distinct actuations. For a single primary fiber under volume expansion, the lengthwise contraction was generated when its helical angle was <~54° (ref. 32). Owing to the surface-wetting properties of CNTs, the infiltration of ethanol into the fiber results in rotation, which is caused by radial expansion and longitudinal contraction. By twisting the primary fibers, the hierarchical structure in the HHF provides a higher capacity for solvent infiltration, resulting in a more rapid and efficient rotation. Upon contact with ethanol, HHFs generate contractive stress with a peak value of 1.5 MPa. This peak value remains almost unchanged when the number of primary fibers is increased from 10 to 40. The generated longitudinal contraction of HHFs reaches up to ~15% (**Fig. 6a–d**). The rotation caused by radial expansion increases from 100 to 2,050 r.p.m. by assembling the primary fibers into HHFs, and a rotary speed of 6,361 r.p.m./m can be achieved (**Table 2**). The rotary actuation of HHFs generates a total work density of 26.7 J/kg (including contraction and rotary outputs), which is 3.5 times higher than that of skeletal muscles[37]. The rotation actuation of HHFs can be tuned by varying the diameter of primary fibers, and the optimum performance can be determined by measuring the revolution speeds of HHFs. For instance, the speed of rotation increased from 2,050 to 2,750 revolutions per meter when the diameter of the primary fiber was decreased from 15 to 10.3 μm. To achieve more substantial contraction movements, the HHF can be further shaped into a left-handed hierarchical spring by a thermo-hydro setting method. The spring generated a large contraction when it was brought into close proximity with the liquid surface of volatilized organic solvents (e.g., ethanol, acetone and

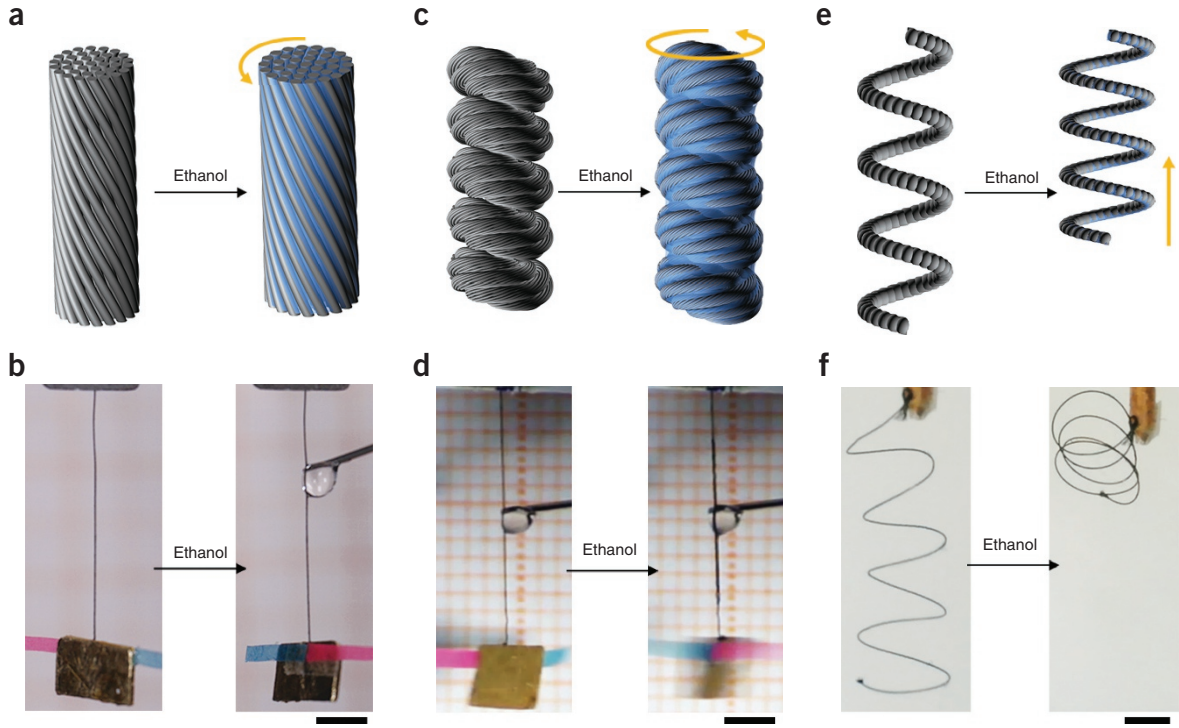

Figure 6 | Actuation performance of helical fibers. (**a**,**b**) Schematic illustration (**a**) and the corresponding photographs (**b**) of the rotary actuation of a single primary fiber with a rotation of 100 r.p.m. Scale bar, 3 mm. (**c**,**d**) Schematic illustration (**c**) and the corresponding photographs (**d**) of the rotary actuation of an HHF with a rotation of 2,050 r.p.m. Scale bar, 3 mm. (**e**,**f**) Schematic illustration (**e**) and the corresponding photographs (**f**) of the contractive actuation in a spring prepared from the HHF with a contractive strain of 60%. Scale bar, 2 cm.

dichloromethane), and the contractive strain reached up to 60% (**Fig. 6e**,**f**). Similarly, elongation actuations could be obtained when the fiber was arranged in a right-handed chirality. The detailed mechanical properties and actuation performances of the HHFs are summarized in **Table 2**.

TABLE 2 | Mechanical properties and actuation performances of the HHFs twisted from 20 primary fibers.

Tensile strength (MPa)	212
Breaking strain (%)	240
Breaking energy (J/g)	74
Contractive stress (MPa)	1.0–1.5
Maximal stress rate (MPa/s)	8.4
Contractive strain (%)	15
Response time (ms)	~44
Maximal strain rate (%)	340
Revolutions (turn per meter)	2,050
Maximal rotary speed (r.p.m./m)	6,361

Note: Any Supplementary Information and Source Data files are available in the online version of the paper.

ACKNOWLEDGMENTS This work was supported by the Ministry of Science and Technology of the People's Republic of China (2016YFA203302 to H.P.), the National Natural Science Foundation of China (21634003, 51573027 to H.P. ; 51403038, 51673043 to X.S.; 21604012 to B.W.) and the Science and Technology Commission of Shanghai Municipality (16JC1400702, 15XD1500400, and 15JC1490200 to H.P.). This work was supported in part by the Samsung Advanced Institute of Technology (SAIT) Global Research Outreach (GRO) Program (IO140919-02248-01).

AUTHOR CONTRIBUTIONS H.P. and X.S. conceived and designed the research project. J.D., Y.X., S.H., P.C., L.B. and Y.H. performed the experiments. J.D., Y.X., S.H., B.W., X.S. and H.P. analyzed the data. J.D., Y.X., S.H., X.S. and H.P. wrote the paper.

COMPETING FINANCIAL INTERESTS The authors declare no competing financial interests.

1. Schulz, M. Speeding up artificial muscles. *Science* **338**, 893–894 (2012).
2. Fratzl, P. & Barth, F.G. Biomaterial systems for mechanosensing and actuation. *Nature* **462**, 442–448 (2009).
3. Bauer, S. *et al.* 25th anniversary article: a soft future: from robots and sensor skin to energy harvesters. *Adv. Mater.* **26**, 149–162 (2014).
4. Madden, J.D. Mobile robots: motor challenges and materials solutions. *Science* **318**, 1094–1097 (2007).
5. Wang, W., Sun, X., Wu, W., Peng, H. & Yu, Y. Photoinduced deformation of crosslinked liquid-crystalline polymer film oriented by a highly aligned carbon nanotube sheet. *Angew. Chem. Int. Ed. Engl.* **51**, 4644–4647 (2012).

© 2017 Macmillan Publishers Limited, part of Springer Nature. All rights reserved.

6. Wu, Z.L. *et al.* Three-dimensional shape transformations of hydrogel sheets induced by small-scale modulation of internal stresses. *Nat. Commun.* **4**, 1586 (2013).
7. Schulgasser, K. & Witztum, A. The hierarchy of chirality. *J. Theor. Biol.* **230**, 281–288 (2004).
8. Fratzl, P. & Weinkamer, R. Nature's hierarchical materials. *Prog. Mater. Sci.* **52**, 1263–1334 (2007).
9. Haines, C.S. *et al.* New twist on artificial muscles. *Proc. Natl. Acad. Sci. USA* **113**, 11709–11716 (2016).
10. Forterre, Y. & Dumais, J. Generating helices in nature. *Science* **333**, 1715–1716 (2011).
11. Egan, P., Sinko, R., LeDuc, P.R. & Keten, S. The role of mechanics in biological and bio-inspired systems. *Nat. Commun.* **6**, 7418 (2015).
12. Elbaum, R., Zaltzman, L., Burgert, I. & Fratzl, P. The role of wheat awns in the seed dispersal unit. *Science* **316**, 884–886 (2007).
13. Armon, S., Efrati, E., Kupferman, R. & Sharon, E. Geometry and mechanics in the opening of chiral seed pods. *Science* **333**, 1726–1730 (2011).
14. Iamsaard, S. *et al.* Conversion of light into macroscopic helical motion. *Nat. Chem.* **6**, 229–235 (2014).
15. Fang, Y., Pence, T.J. & Tan, X. Fiber-directed conjugated-polymer torsional actuator: nonlinear elasticity modeling and experimental validation. *IEEE ASME Trans. Mechatron.* **16**, 656–664 (2011).
16. Mirvakili, S.M. *et al.* Niobium nanowire yarns and their application as artificial muscles. *Adv. Funct. Mater.* **23**, 4311–4316 (2013).
17. Mirfakhrai, T. *et al.* Electrochemical actuation of carbon nanotube yarns. *Smart Mater. Struct.* **16**, S243 (2007).
18. Sun, X. *et al.* Unusual reversible photomechanical actuation in polymer/nanotube composites. *Angew. Chem. Int. Ed. Engl.* **51**, 8520–8524 (2012).
19. Liu, Z. *et al.* Hierarchically buckled sheath-core fibers for superelastic electronics, sensors, and muscles. *Science* **349**, 400–404 (2015).
20. Guo, W. *et al.* A novel electromechanical actuation mechanism of a carbon nanotube fiber. *Adv. Mater.* **24**, 5379–5384 (2012).
21. Chen, P. *et al.* Biologically inspired, sophisticated motions from helically assembled, conducting fibers. *Adv. Mater.* **27**, 1042–1047 (2015).
22. Haines, C.S. *et al.* Artificial muscles from fishing line and sewing thread. *Science* **343**, 868–872 (2014).
23. Wang, J.-S. *et al.* Hierarchical chirality transfer in the growth of Towel Gourd tendrils. *Sci. Rep.* **3**, 3102 (2013).
24. Chen, P. *et al.* Hierarchically arranged helical fibre actuators driven by solvents and vapours. *Nat. Nanotech.* **10**, 1077–1083 (2015).
25. He, S. *et al.* A mechanically actuating carbon-nanotube fiber in response to water and moisture. *Angew. Chem. Int. Ed. Engl.* **54**, 14880–14884 (2015).
26. Li, Y. *et al.* Overtwisted, resolvable carbon nanotube yarn entanglement as strain sensors and rotational actuators. *ACS Nano* **7**, 8128–8135 (2013).
27. Zhang, Y. *et al.* Flexible and stretchable lithium-ion batteries and supercapacitors based on electrically conducting carbon nanotube fiber springs. *Angew. Chem. Int. Ed. Engl.* **126**, 14564–14568 (2014).
28. De Volder, M.F.L., Tawfick, S.H., Baughman, R.H. & Hart, A.J. Carbon nanotubes: present and future commercial applications. *Science* **339**, 535–539 (2013).
29. Li, D. *et al.* Molecular, supramolecular, and macromolecular motors and artificial muscles. *MRS Bull.* **34**, 671–681 (2009).
30. Jiang, K., Li, Q. & Fan, S. Nanotechnology: spinning continuous carbon nanotube yarns. *Nature* **419**, 801–801 (2002).
31. Baughman, R.H. *et al.* Carbon nanotube actuators. *Science* **284**, 1340–1344 (1999).
32. Foroughi, J. *et al.* Torsional carbon nanotube artificial muscles. *Science* **334**, 494–497 (2011).
33. Qiu, J. *et al.* Liquid infiltration into carbon nanotube fibers: effect on structure and electrical properties. *ACS Nano* **7**, 8412–8422 (2013).
34. Meng, F., Zhao, J., Ye, Y., Zhang, X. & Li, Q. Carbon nanotube fibers for electrochemical applications: effect of enhanced interfaces by an acid treatment. *Nanoscale* **4**, 7464–7468 (2012).
35. Fang, X. *et al.* Core-sheath carbon nanostructured fibers for efficient wire-shaped dye-sensitized solar cells. *Adv. Mater.* **26**, 1694–1698 (2014).
36. Skotheim, J.M. & Mahadevan, L. Physical limits and design principles for plant and fungal movements. *Science* **308**, 1308–1310 (2005).
37. Mirfakhrai, T., Madden, J.D. & Baughman, R.H. Polymer artificial muscles. *Mater. Today* **10**, 30–38 (2007).